Available online at www.sciencedirect.com

ScienceDirect

Geochimica et Cosmochimica Acta 325 (2022) 170–186

Geochimica et Cosmochimica Acta

www.elsevier.com/locate/gca

Oxygen isotopes of calcite precipitated at high ionic strength: $CaCO_3$-DIC fractionation and carbonic anhydrase inhibition

Ellen K. Olsen [a,*], James M. Watkins [a], Laurent S. Devriendt [a,b]

[a] Department of Earth Sciences, University of Oregon, Eugene, OR, United States
[b] Department of Ocean Systems, NIOZ Royal Netherlands Institute for Sea Research, and Utrecht University, Texel, the Netherlands

Received 20 October 2021; accepted in revised form 27 January 2022; Available online 4 February 2022

Abstract

Background electrolytes affect calcite precipitation and dissolution rates and hence have the potential to impact kinetic isotope fractionation between calcite and the dissolved inorganic carbon (DIC) species. We grew inorganic calcite from NaCl-$CaCl_2$ solutions ($T = 25$ °C, pH = 8.3, and crystal growth rate = $10^{-6.3 \pm 0.3}$ mol m^{-2} s^{-1}) to test for potential ionic strength effects on the oxygen isotope fractionation between calcite and an isotopically equilibrated inorganic carbon pool ($\alpha_{c/EIC}$). Calcite was grown in the presence of the enzyme carbonic anhydrase from bovine erythrocytes (bCA) to promote isotopic equilibration of the DIC pool.

No evidence of an ionic strength effect on $\alpha_{c/EIC}$ was found for NaCl concentrations up to 0.35 M ($1000\ln\alpha_{c/w} = 28.0 \pm 0.1$; $n = 7$). For experiments conducted with [NaCl] > 0.35 M, the DIC pool could not be maintained in isotopic equilibrium with water due to the inhibitory effect of NaCl on bCA. The use of other types of CA may be required to maintain isotopic equilibration of DIC in solution with ionic strength close to or above that of seawater.

The oxygen isotope results were modeled successfully with an isotopic box model for a CO_2-fed solution that tracks the isotopic composition of each DIC species and $CaCO_3$. The experimental and modeling results suggest that the efficacy of bCA decreases exponentially with increasing [NaCl]. We quantify the salt effect on the quantity k_{cat}/K_M, which relates the catalyzed rate constant for CO_2 hydration to the concentration of bCA. The salt effect can be implemented in models of biomineralization with potential to extend our knowledge of oxygen isotope vital effects in marine organisms.

Keywords: Oxygen isotopes; Calcite; Kinetic isotope effects; Carbonic anhydrase

1. INTRODUCTION

Laboratory-controlled calcite and aragonite precipitation experiments have been used to determine isotopic fractionation factors between carbonate minerals and dissolved carbonate species or water. When crystals grow slowly, near chemical equilibrium conditions, oxygen isotope partitioning is expected to depend solely on temperature, providing a theoretical foundation for oxygen isotope thermometry (Bigeleisen and Mayer, 1947; Urey, 1947). It is often the case, however, that crystals grow fast enough that isotopic exchanges between phases do not reach equilibrium, leading to kinetic isotopic effects (KIEs) that depend on variables other than temperature and arise from either or both of the following: (1) a dissolved inorganic carbon ($DIC = CO_2 + HCO_3^- + CO_3^{2-}$) pool that is not fully equilibrated with water (Usdowski et al., 1991; Zeebe and Wolf-Gladrow, 2001; Devriendt et al., 2017b) and/or

* Corresponding author.
E-mail address: eolsen2@uoregon.edu (E.K. Olsen).

https://doi.org/10.1016/j.gca.2022.01.028
0016-7037/

(2) transport of ions to and from the mineral surface and reaction of ions at the mineral surface (DePaolo, 2011; Watkins et al., 2014, 2017).

Until recently, it was difficult to separate these two different sources of KIEs. The enzyme carbonic anhydrase from bovine erythrocytes (bCA) is commercially available and can be used in carbonate precipitation experiments to reduce or eliminate KIEs arising from homogeneous chemical reactions between DIC species and water (Uchikawa and Zeebe, 2012; Watkins et al., 2013, 2014). Addition of bCA in calcite growth experiments is useful for investigating isotopic fractionations under conditions that mimic the secretion of biogenic carbonates and for isolating surface reaction-controlled KIEs.

In the few calcite growth experiments where bCA has been employed for the purpose of equilibrating the DIC pool, there is a resolvable pH- and growth rate-dependence to the KIEs (Watkins et al., 2013, 2014). This suggests that surface reaction-controlled kinetic effects may be sensitive to the proportion of HCO_3^- versus CO_3^{2-} participating in growth (pH effect) and there is a mass dependence to the reaction rate constants (growth rate effect) for the reactions:

$$Ca^{2+} + HCO_3^- \underset{k_b}{\overset{k_f}{\rightleftarrows}} CaCO_3 + H^+ \quad (1)$$

and

$$Ca^{2+} + CO_3^{2-} \underset{k_b}{\overset{k_f}{\rightleftarrows}} CaCO_3 \quad (2)$$

where the k_f's and k_b's are forward (precipitation) and backward (dissolution) rate constants, respectively.

Previous experiments with bCA were done in low ionic strength solutions, but background electrolytes are known to affect the solubility product of calcite (Mucci, 1983), calcite growth and dissolution kinetics (Ruiz-Agudo et al., 2010, 2011; Hong and Teng, 2014), calcite growth morphology (Wang et al., 2011), and solution speciation (e.g. Millero et al., 2006, 2007). Hence, solution composition may influence KIEs and be partly responsible for oxygen isotope variability in natural carbonates.

Here, we performed calcite-growth experiments under constant temperature (25 °C) and pH (8.3) but with distinct salinities ($0.0 < [NaCl] < 1.4$ M; I = 0.1–1.6) to assess the effect of ionic strength on calcite-DIC oxygen isotope fractionation and on the activity of bCA. We found no evidence for a salinity effect on the oxygen isotope fractionation between calcite and the DIC species up to a NaCl concentration of ~0.35 M. However, NaCl significantly lowers the activity of the enzyme bCA, giving rise to highly variable isotopic results at higher NaCl concentrations. We use these well-controlled experiments to adapt and refine a previously published isotopic box model for kinetic isotope effects in the $CaCO_3$-DIC-H_2O system (Chen et al., 2018; Christensen et al., 2021). The model is used to constrain the functional form for the salt effect on the enzyme-catalyzed rate constant for CO_2 hydration.

2. METHODS

2.1. Calcite growth experiments

We use the same experimental setup as Watkins et al. (2013, 2014). Although the methods were described previously, we review them here because the details are used to develop a quantitative model reflecting our experimental conditions (Section 4). We measured the $\delta^{18}O$ of input CO_2, which matters if the DIC pool is not fully isotopically equilibrated, and monitored [DIC] and total alkalinity 2–4 times per day.

Solutions were prepared by dissolving $CaCl_2{\cdot}2H_2O$ (30 mM), NH_4Cl (5 mM) and variable amounts of NaCl (0–1.4 M) in 1.7 L of deionized water. The beaker with the prepared solutions was submerged in a water bath containing both heating and cooling elements for precise temperature control (25 ± 0.2 °C). The beaker was sealed by a lid that has ports for a pH probe, NaOH dripper, sampling syringe, and gas bubbler (Watkins et al., 2013). DIC was added to the solution by continuous bubbling of a CO_2-in-N_2 gas mixture through a diffusion stone at 0.5 standard cubic feet per hour using a SmartTrak100 gas flow controller (Sierra Instruments). The pCO_2 of the headspace was recorded by a K-30 USB CO_2 Probe Data Logger (CM0039 from CO_2meter.com).

Prior to the start of an experiment, the gas was fluxed through the solution for 1–6 hours, during which time the headspace pCO_2 decreased from ~500 ppm to 240–280 ppm as the lab air was replaced by the gas tank mixture.

To begin an experiment, the autotitrator was activated and between 0.3–1.2 mL of 1 M NaOH was dispensed to bring the pH up to a setpoint of 8.3 ± 0.02. The increase in pH caused CO_2 from the bubbles to partition into solution, which led to an abrupt decrease in the pCO_2 of the headspace. Variable amounts of bCA (0–3 μM) were added after the solution had reached a pH of 8.3. The total alkalinity (TA) as measured by Gran titration increased from 0 to ~0.2–0.7 mEq/L following the addition of NaOH. The TA was measured each time samples were collected for [DIC] during the course of an experiment. From 22 titrations of the same solution carried out over the course of one week, we determined a 95% confidence interval of ±0.03 and a standard error of 0.003 for our reported TA values, which accounts for any error due to pH probe calibration drift, issues with the autotitrator dispensing HCl accurately, and subjectivity in the Gran method calculation.

All of our experiments behaved similarly to the example shown in Fig. 1a. Each experiment had a pre-precipitation period (Stage I) during which DIC, TA, and pCO_2 of the headspace increased as CO_2 dissolved in solution. Eventually, enough DIC was added for calcite crystals to nucleate and grow on the beaker walls, marking the onset of the calcite precipitation period (Stage II). The duration of Stages I and II, as well as the rate of NaOH addition, varies somewhat between experiments (Fig. 1b), which we attribute to fluctuations in the average size of bubbles emanating from the diffusion stone and random nucleation processes leading to differences in the initial surface area of the first crys-

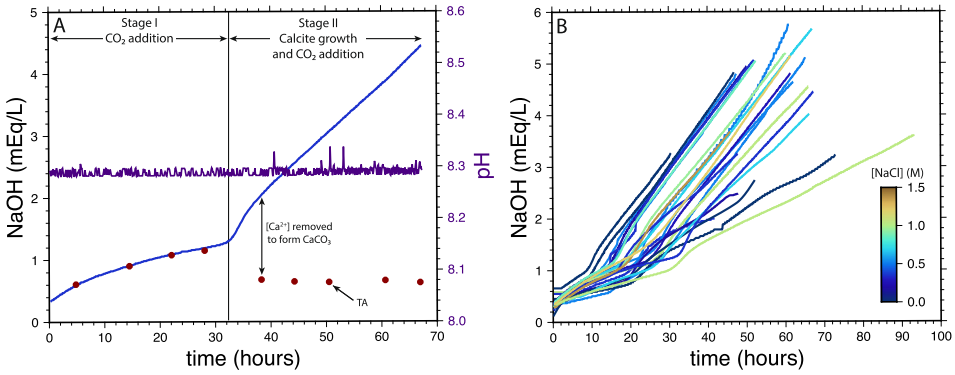

Fig. 1. Behavior of the calcite growth experiments. (A) Example of an experimental run (S11). During Stage I, the increase in TA matches the amount of NaOH added to offset the addition of CO_2 to solution. At the onset of Stage II, the change in TA is due to addition of NaOH as well as removal of Ca^{2+} to $CaCO_3$. During Stage II, the difference between NaOH added and TA can be used to calculate the $CaCO_3$ flux (mmol/h). (B) Rate of NaOH addition for all experiments. The range of slopes during Stage II translates to a range in the $CaCO_3$ precipitation rate from 0.04 to 0.15 mmol/h.

tals. The growth rate of calcite (mmol/h) was calculated from the rate of NaOH addition during Stage II (cf. Watkins et al., 2013).

The TA and [DIC] were measured at regular intervals and results from all experiments are plotted together in Fig. 2a and b. Solution ionic strength and free activities of Ca^{2+} and CO_3^{2-} were calculated through the R-package of PHREEQC using the Pitzer database (Charlton and Parkhurst, 2011; De Lucia and Kühn, 2013). The degree of supersaturation (Fig. 2c, $\Omega = (a_{Ca^{2+}} \cdot a_{CO_3^{2-}})/K_{sp}$) was determined by using these ionic activities and the solubility product of calcite at 25 °C ($K_{sp} = 10^{-8.42}$, Jacobson and Langmuir, 1974). Additional considerations regarding DIC speciation as a function of salinity and solution composition are provided in Supplement S1. In all experiments, a short period of rapid crystal growth at high Ω (5–11) was followed by a long period of crystal growth under relatively steady conditions at $\Omega = 3.7 \pm 1.5$.

Following the final measurements, experimental solutions were discarded and crystals adhered to the beaker walls were rinsed 3 times with de-ionized water and allowed to air-dry. Precipitates from each experiment were imaged on the FEI Quanta 200 Environmental Scanning Electron Microscope (ESEM) at the Center for Advanced Materials Characterization (CAMCOR) at the University of Oregon. ESEM imaging found only rhombohedral to rhombo-scalenohedral $CaCO_3$ crystals present. Additionally, X-Ray Diffraction (XRD) analysis of select experiments spanning the range in [NaCl] conducted at the Oregon State University X-Ray Diffraction Facility confirmed that calcite is the only phase present.

2.2. $\delta^{18}O$, $\delta^{13}C$, and [DIC] measurements

Exetainers for all experimental water samples were prepared on a GasBench II in the Stable Isotope Laboratory at the University of Oregon, by flushing them with helium gas for five minutes. The isotopic composition of CO_2 in the CO_2-in-N_2 mixtures (Table 1) was measured in the Stable Isotope Lab at the University of Oregon after cryogenic separation from the N_2 gas on a vacuum line that is otherwise and usually used for mineral fluorination. The gas tank with a regulator was connected to the inlet port of the vacuum line and set to 1 bar gauge pressure. Gas was allowed to flow into the line and atmospheric air was flushed out by cyclical opening and closing of valves at least three times to completely fill the line with the CO_2-in-N_2 gas mixture and exclude air. Dewar flasks containing liquid nitrogen (LN_2) were placed at three traps along the line for at least 20 minutes to allow the small proportion of CO_2 in the gas mixture to freeze. The N_2 in the line was pumped away, and then LN_2 dewars at the two upstream traps were removed and heated to allow the CO_2 to collect at the yield measurement trap that was still submerged in LN_2. Yield was obtained by heating the last and third trap that was isolated between valves, and observing the pressure on a digital manometer. An initial low digital gauge pressure reading was common due to the small fraction of CO_2 present in the gas (typically 200 ppm), often necessitating multiple cycles of gas mixture inlet and freezing of CO_2 at the traps. After all the upstream valves were closed, the last LN_2 dewar was removed, the trap heated, and downstream valve opened, allowing the purified CO_2 to flow from the vacuum line to a Thermo-Finnigan MAT 253 mass spectrometer.

The isotopic composition of the sample CO_2 gas was measured using the mass spectrometer dual inlet system, and a CO_2 reference gas of known composition. Though the standard analytical error (1σ) is ±0.010‰ for $\delta^{18}O$ and ±0.005‰ for $\delta^{13}C$, we suggest that our analyses may have greater uncertainty for several other reasons. Isotopic fractionation could be occurring at the gas tank regulator as the gas flows from the tank into the fluorination line, as well as during the preferential freezing of isotopically heavy CO_2. Additionally, cryogenic separation procedures and mass spectrometer analyses suggest that some of our CO_2-in-N_2 gas tanks contained a small amount of H_2O, which decreases our confidence in the measurements.

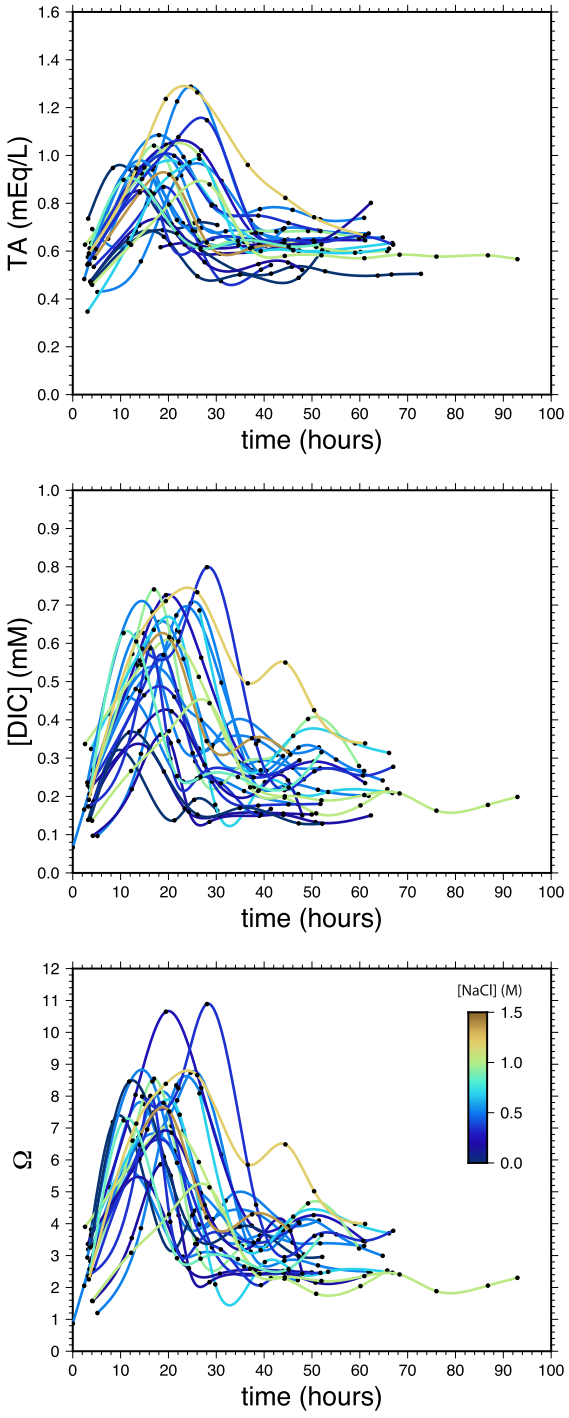

Fig. 2. Variations in total alkalinity (TA, A), dissolved inorganic carbon (DIC, B) and calcite saturation state (Ω, C) during the course of each calcite growth experiment. Black dots are measured points (or calculated from measured points) and curves are splines. This figure shows the variabilities in TA, DIC and Ω are not related to the different NaCl concentrations. Typically, Ω increased to between 5 and 9 around the 15–20 h mark before decreasing to a quasi-steady state value of Ω = 2–4 after 30 h.

Taking these uncertainties into account, we conclude the isotopic analysis of our CO_2 gas to be within ±1‰, which is sufficiently accurate for our purposes.

The isotopic composition of calcite, aqueous solution, and DIC were analyzed at the Stable Isotope Laboratory in the College of Earth, Ocean, and Atmospheric Sciences (CEOAS) at Oregon State University. Data are presented in standard delta notation. Water samples for DIC and $\delta^{13}C$ were taken 2–4 times per day during an experiment, while water for $\delta^{18}O$ was taken only at the end of most experiments since previous work showed constant $\delta^{18}O$ values over the course of an experiment (Baker, 2015).

For DIC analysis, 3.5 mL of water was injected through rubber septa into He-flushed exetainers. At CEOAS, 0.1 mL of 85% orthophosphoric acid was added to the exetainers. After equilibrating for 4 hours, the gas headspace was analyzed by continuous-flow mass spectrometry on a GasBench-DeltaV system. A known concentration in-house $NaHCO_3$ standard was analyzed with the samples, from which a calibration curve was determined and DIC concentration in our samples was approximated. Data are reported in standard delta notation relative to VPDB (Supplement Table S3.2). The standard analytical error (1σ) is ± 0.15‰ for $\delta^{13}C$ of DIC.

Water samples for $\delta^{18}O$ were collected in He-flushed exetainers and filled almost completely (~11 mL) to minimize headspace and allow for replicate analyses. The $\delta^{18}O$ was analyzed using the CO_2-equilibration method whereby the CO_2 headspace is equilibrated with 5 mL of water while agitated in an 18 °C water bath. The CO_2 was then analyzed by dual inlet mass spectrometry on a DeltaPlus XL and data are reported in standard delta notation relative to VSMOW (Table 1). The standard analytical error (1σ) is ± 0.05‰ for $\delta^{18}O$ of H_2O.

Calcite samples were reacted with 105% orthophosphoric acid in a Kiel III preparation device for 8 minutes at 70 °C. Evolved CO_2 and H_2O gases were condensed and CO_2 was separated and transferred into a MAT 252 mass spectrometer for analysis via dual inlet mass spectrometry. Data are reported in standard delta notation relative to VPDB (Table 1). The $\delta^{18}O$ data were converted to the VSMOW scale by the following relationship: $\delta^{18}O_{VSMOW} = 1.03091 \cdot \delta^{18}O_{VPDB} + 30.91$ (Coplen et al., 1983). The standard analytical error (1σ) is ± 0.05‰ for $\delta^{18}O$ and ± 0.03‰ for $\delta^{13}C$.

3. RESULTS

3.1. Oxygen isotope fractionation

The fractionation factor between two phases or compounds, for example calcite (c) and water (w), are related to delta values as follows:

$$\alpha_{c/w} = \frac{(^{18}O/^{16}O)_c}{(^{18}O/^{16}O)_w} = \frac{\delta^{18}O_c + 1000}{\delta^{18}O_W + 1000}. \quad (3)$$

With [NaCl] = 0 and [bCA] ≥ 0.2 μM, the data form a tight cluster ($1000\ln\alpha_{c/w} = 28.0 \pm 0.1$‰, $n = 4$, Table 1, Fig. 3) that agrees with previous results from calcite growth experiments carried out at 25 °C, pH 8.3 and with bCA (Watkins et al., 2013, 2014; Baker, 2015). These experiments indicate 0.2 μM bCA is sufficient to maintain an isotopically equilibrated DIC pool in low salinity experiments.

Table 1
Experimental parameters and isotopic data for all experiments of this study.

Experiment	[NaCl] (M)	Salinity (g/kg)[a]	bCA (mg)	[bCA] (μM)	R (mmol/h)	$\log_{10}R$ (mol/m^2/s)	$\delta^{18}O_{gas}$ CO_2 (VSMOW)	$\delta^{18}O_w$ (VSMOW)	$\delta^{18}O_c$ (VPDB)	$\delta^{18}O_c$ (VSMOW)	$1000\ln\alpha_{c\text{-}w}$
S2[b]	0.52	35	11.35	0.22	-	-	12.89	−11.65	−16.39	14.02	25.64
S3[b]	0.52	35	10.48	0.21	-	-	12.89	−11.52	−16.43	13.98	25.47
S4[b]	0.18	15	10.06	0.20	-	-	12.89	−11.42	−14.24	16.23	27.59
S5	0.35	25	10.89	0.21	0.053	−6.10	12.89	−11.32	−14.34	16.13	27.38
S6	0	3.5	10.6	0.21	0.044	−6.45	12.74	−11.31	−13.66	16.83	28.06
S7	0.18	15	10.04	0.20	0.057	−6.20	12.74	−11.34	−14.34	16.13	27.40
S8	0	3.5	10.48	0.21	0.053	−6.27	12.74	−11.39	−13.84	16.65	27.96
S9	0.35	25	10.21	0.20	0.070	−6.24	12.74	−11.40	−15.95	14.47	25.83
S10	0.69	45	10	0.20	0.071	−6.34	12.74	−11.39	−16.52	13.88	25.24
S11	0.35	25	10.01	0.20	0.093	−6.27	12.74	−11.62	−16.51	13.89	25.48
S12	1.37	85	10.03	0.20	0.094	−6.17	22.20	−11.57	−16.06	14.36	25.89
S13	1.03	65	10.27	0.20	0.040	−6.54	22.20	−11.72	−15.61	14.82	26.50
S14	0.86	55	10.24	0.20	0.103	−6.30	22.20	−11.82	−16.62	13.78	25.57
S15	1.20	75	10.41	0.20	0.101	−6.31	22.20	−11.82	−16.21	14.20	25.99
CA1	0.52	35	0	0	0.101	−6.31	24.30	−11.83	−16.01	14.41	26.20
CA2	0.52	35	20.35	0.40	0.102	−6.26	24.30	−11.86	−15.84	14.58	26.40
CA3	0.52	35	0.97	0.02	0.102	−6.27	24.30	−11.91	−16.43	13.98	25.86
CA4	0	3.5	0	0	0.101	−6.07	24.30	−11.68	−16.72	13.68	25.33
CA5	0.52	35	50.13	0.98	0.090	−6.31	24.30	−11.17	−14.18	16.29	27.39
CA6	0.52	35	100	1.96	0.105	−6.34	24.30	−11.18	−14.16	16.31	27.42
CA7	0.26	20	50	0.98	0.095	−6.30	24.30	−11.33	−13.67	16.82	28.07
CA9	0.95	60	100	1.96	0.089	−6.37	13.45	−11.57	−15.93	14.49	26.02
CA12	0.69	45	75.82	1.49	0.085	−6.44	13.45	−11.76	−14.91	15.54	27.24
CA13	1.03	65	150	2.94	0.082	−6.35	13.45	−11.65	−15.21	15.24	26.84
CA14	0.18	15	49.01	0.96	0.101	−6.29	13.45	−11.85	−14.16	16.31	28.09
CA15	0.35	25	50	0.98	0.100	−6.31	13.45	−11.86	−14.16	16.31	28.11
CA18[c]	0	3.5	20	0.39	0.152	−6.28	23.50	−11.88	−14.26	16.21	28.03
CA20	0	3.5	10.12	0.20	0.089	−6.34	13.63	−11.95	−14.34	16.12	28.02

[a] Salinities given are approximate.
[b] Calcite growth rate could not be calculated for early experiments due to use of an unreliable NaOH autotitrator.
[c] CA18 used an 800 ppm CO_2-in-N_2 gas tank, while all other experiments used 200 ppm CO_2-in-N_2 tanks. Flow rate was scaled back so that all experiments have a constant flux of 0.12–0.13 mmol CO_2/h.

Results from experiments with added NaCl (0.2–1.4 M) and [bCA] ~ 0.2 μM vary from 25.2 to 27.6‰ in $1000\ln\alpha_{c/w}$ (Table 1, Fig. 3) and are comparatively lower than results from the low salinity experiments.

Repeat NaCl experiments but with higher bCA concentrations (up to 2.9 μM) display $1000\ln\alpha_{c/w}$ values consistently higher than those from experiments with [bCA] ~ 0.2 μM, indicating higher [bCA] are required for isotopic equilibration of the DIC pool in solutions of high ionic strength. Specifically, experiments with [NaCl] from 0.18 to 0.35 M and [bCA] ~ 1 μM resulted in $1000\ln\alpha_{c/w}$ values (28.1 ± 0.05‰) indistinguishable from the low salinity experiments (28.0 ± 0.1‰). These results suggest that, for these experiments, (1) the DIC pool remained isotopically equilibrated with ~1 μM of bCA and (2) [NaCl] of up to 0.35 M has no significant effect on $1000\ln\alpha_{c/w}$. However, experiments with [NaCl] > 0.35 M resulted in $1000\ln\alpha_{c/w}$ values significantly lower than 28.0‰ despite very high [bCA] (up to 2.9 μM). The cause of the lower $1000\ln\alpha_{c/w}$ values at high ionic strength is investigated in Section 6.2.

4. MODEL FOR CALCITE GROWTH FROM A DIC POOL WITH VARIABLE LEVEL OF ISOTOPIC EQUILIBRATION

The variability in $1000\ln\alpha_{c/w}$ as a function of [bCA] is a manifestation of kinetic effects arising from a variably equilibrated DIC pool. Recent progress has been made on the development of numerical models that quantify kinetic isotope effects in the $CaCO_3$-DIC-H_2O system (Chen et al., 2018; Christensen et al., 2021; Uchikawa et al., 2021). In this section, we present a model adapted from that of Chen et al. (2018), and use it to evaluate the oxygen isotopic variations observed. This is aided by the constraints we have on the CO_2 flux, $\delta^{18}O$ of CO_2 gas, and carbonate growth rates.

We begin with a 1.7 L solution at 25 °C, pH = 8.3, $[Ca^{2+}] = 30$ mM and [DIC] ~ 0.01 mM. The DIC is initially isotopically equilibrated. Equilibrium fractionation factors used in the model are provided in Table 2. As CO_2 bubbles through, some of it partitions into solution, constituting a net flux of $CO_{2(aq)}$ (i.e., DIC). The incoming $CO_{2(g)}$ has the isotopic composition of the gas tank, which is out of equilibrium with the dissolved $CO_{2(aq)}$ and water. We assume there is no isotopic fractionation of CO_2 as it gets converted from the gaseous to dissolved state (equilibrium fractionation between $CO_{2(g)}$ and $CO_{2(aq)}$ < 0.2‰, Brenninkmeijer et al., 1983; Beck et al., 2005; diffusive isotope effects < 0.7‰; O'Leary, 1984). The CO_2 that enters solution undergoes hydration and hydroxylation reactions to produce HCO_3^-, a fraction of which deprotonates to form CO_3^{2-}. As the concentration of CO_3^{2-} increases, the degree of supersaturation (Ω) also increases, and calcite grows at a rate that depends on the degree of supersaturation. Fast calcite growth draws down [DIC], thus slowing calcite growth in a negative feedback.

For the model to be informative, it should: (1) capture the behavior that a quasi-steady state is reached in the system whereby the influx of DIC from CO_2 (F_{CO2}) is balanced by the outflux of DIC to calcite (F_{CaCO3}), (2) reach steady state fluxes that agree with the inferred growth rate (mmol/h), and (3) provide insights into the isotopic results. For this latter point, we specifically seek to explain the 3‰ variability among the experiments despite the use of high [bCA].

4.1. Chemical reactions

The model tracks the following chemical and isotope exchange reactions (Chen et al., 2018; Christensen et al., 2021):

$$CO_2 + H_2O \underset{k_{-1}}{\overset{k_{+1}}{\rightleftarrows}} HCO_3^- + H^+, \tag{4}$$

$$CO_2 + OH^- \underset{k_{-4}}{\overset{k_{+4}}{\rightleftarrows}} HCO_3^-, \tag{5}$$

$$CO_2 + H_2^{18}O \underset{1/3a_{-1}}{\overset{a_{+1}}{\rightleftarrows}} HC^{18}OO_2^- + H^+, \tag{6}$$

$$CO_2 + {}^{18}OH^- \underset{1/3a_{-4}}{\overset{a_{+4}}{\rightleftarrows}} HC^{18}OO_2^-, \tag{7}$$

$$C^{18}OO + H_2O \underset{2/3b_{-1}}{\overset{b_{+1}}{\rightleftarrows}} HC^{18}OO_2^- + H^+, \tag{8}$$

and

$$C^{18}OO + OH^- \underset{2/3b_{-4}}{\overset{b_{+4}}{\rightleftarrows}} HC^{18}OO_2^-. \tag{9}$$

The k's are rate constants for the (de)hydration and (de)hydroxylation reactions. Rate constants for the ^{18}O-substituted species are denoted a or b, with a representing substitution on H_2O or OH^-, and b representing substitution on CO_2. The ratio of these rate constants is equal to the equilibrium constant for each reaction, as given in Table 3.

We solve numerically these five coupled ordinary differential equations:

$$\frac{d[CO_2]}{dt} = -k_{+1}[CO_2] + k_{-1}[EIC]\chi[H^+] - k_{+4}[CO_2][OH^-] + k_{-4}[EIC]\chi + \frac{F_{CO_2}}{V} \tag{10}$$

$$\frac{d[EIC]}{dt} = k_{+1}[CO_2] - k_{-1}[EIC]\chi[H^+] + k_{+4}[CO_2][OH^-] - k_{-4}[EIC]\chi - \frac{F_{CaCO_3}}{V} \tag{11}$$

$$\frac{d[C^{18}OO]}{dt} = -b_{+1}[C^{18}OO] + \frac{2}{3}b_{-1}[{}^{18}EIC]\,{}^{18}\chi[H^+] - b_{+4}[C^{18}OO][OH^-] + \frac{2}{3}b_{-4}[{}^{18}EIC]\,{}^{18}\chi + \frac{F_{CO_2}\,{}^{18}R_{CO_2}}{V} \tag{12}$$

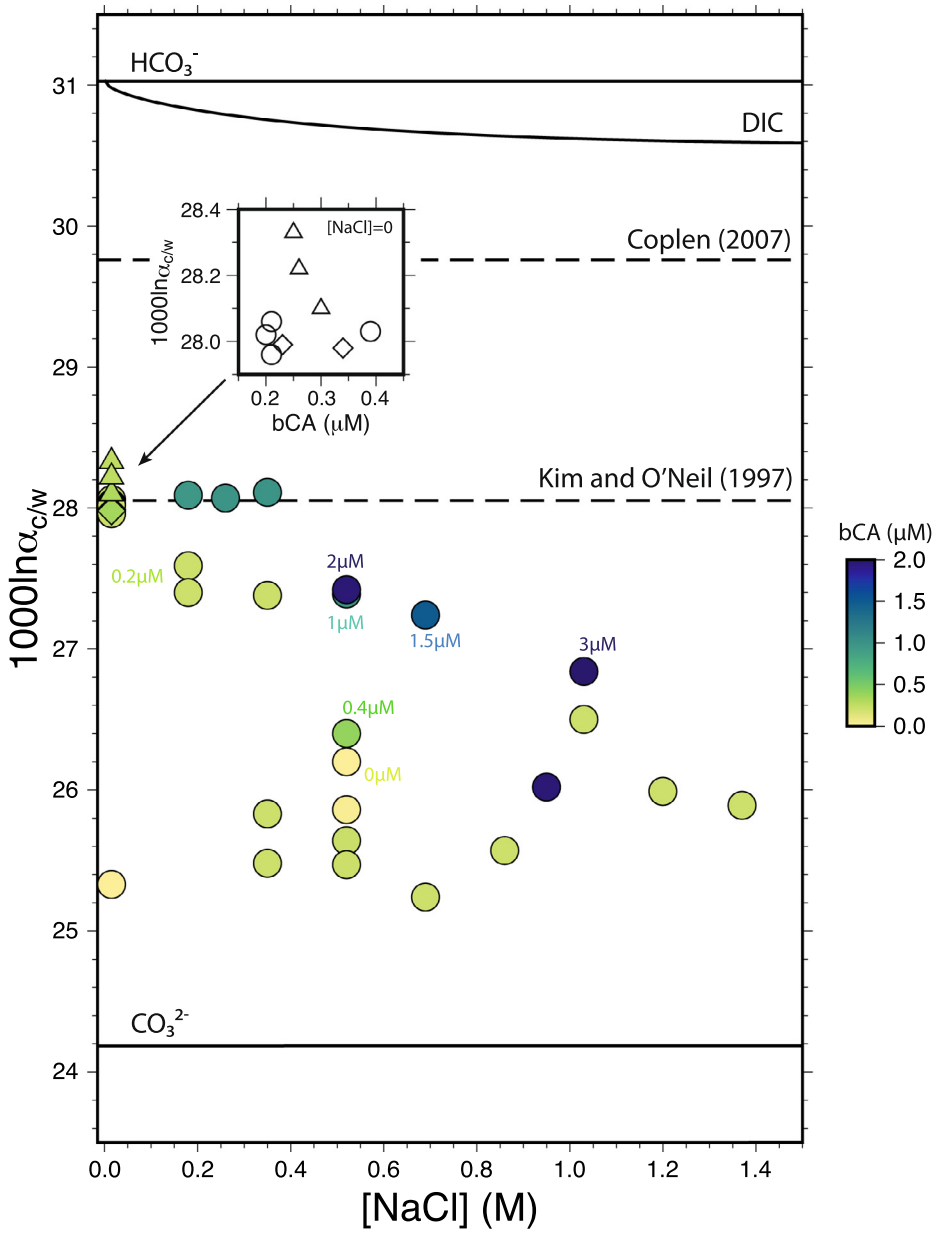

Fig. 3. Calcite-water oxygen isotope fractionation expressed as $1000\ln\alpha_{c/w}$. Results from this study's experiments (circles) at low salinity ([NaCl] = 0, $n = 4$) agree with previous calcite growth experiments conducted at pH 8.3 and 25 °C with bovine carbonic anhydrase (Watkins et al., 2014 – triangles; Baker, 2015 – diamonds), as well as with the expected value obtained using the Kim and O'Neil (1997) calibration. Experiments with [NaCl] > 0.35 M show lower and variable $1000\ln\alpha_{c/w}$ despite the use of high bovine carbonic anhydrase concentrations. Equilibrium fractionation factors are listed in Table 2 (Beck et al., 2005; Coplen, 2007). We use the Zeebe (2007) expression to calculate oxygen isotope fractionation between the sum of DIC and water, substituting Millero et al. (2007) *p*K values for simple NaCl solutions and equilibrium fractionation factors from Beck et al. (2005).

Table 2
Compilation of equilibrium fractionation factors (EFFs; T in Kelvin).

Compounds	Equation	α (25 °C)	References
$CO_{2(g)}$–H_2O	$17.611\ T^{-1} + 0.9821$	1.0412	Zeebe (2007)
$CO_{2(aq)}$–H_2O	$\exp(2520\ T^{-2} + 0.01212)$	1.0413	Beck et al. (2005)
HCO_3^-–H_2O	$\exp(2590\ T^{-2} + 0.00189)$	1.0315	Beck et al. (2005)
CO_3^{2-}–H_2O	$\exp(2390\ T^{-2}\text{-}0.00270)$	1.0245	Beck et al. (2005)
Calcite-H_2O	$\exp\left(\frac{17747}{T} - 29.777}{1000}\right)$	1.0302	Coplen (2007), Watkins et al. (2013)
OH^-–H_2O	$(1+\left[-4.4573 + \frac{10.3255 \cdot 10^3}{T} - \frac{0.5976 \cdot 10^6}{T^2}\right]/1000)^{-1}$	0.9771	Zeebe (2020)

$$\frac{d[^{18}\mathrm{EIC}]}{dt} = a_{+1}[\mathrm{CO_2}]r_w - \frac{1}{3}a_{-1}[^{18}\mathrm{EIC}]\,{}^{18}\chi[\mathrm{H^+}] + a_{+4}[\mathrm{CO_2}][^{18}\mathrm{OH^-}] - \frac{1}{3}a_{-4}[^{18}\mathrm{EIC}]\,{}^{18}\chi + b_{+1}[\mathrm{C^{18}OO}] - \frac{2}{3}b_{-1}[^{18}\mathrm{EIC}]\,{}^{18}\chi[\mathrm{H^+}] + b_{+4}[\mathrm{C^{18}OO}][\mathrm{OH^-}] - \frac{2}{3}b_{-4}[^{18}\mathrm{EIC}]\,{}^{18}\chi - \frac{F_{\mathrm{CaCO_3}}}{\mathrm{V}}\frac{[^{18}\mathrm{EIC}]}{[\mathrm{EIC}]}\alpha_{c/\mathrm{EIC}} \quad (13)$$

and

$$\frac{d[\mathrm{Ca^{2+}}]}{dt} = -\frac{F_{\mathrm{CaCO_3}}}{\mathrm{V}} \quad (14)$$

where F_{CO2} and F_{CaCO3} are fluxes (moles s^{-1}), V is volume (L), and HCO_3^- and CO_3^{2-} are written together as EIC (short for "equilibrated inorganic carbon"), assuming instantaneous equilibrium between these two species (Chen et al., 2018). The factors of 1/3 and 2/3 are needed for oxygen isotope mass balance; for every mole of $HC^{18}OO_2^-$ that undergoes dehydrations, ~2/3 goes to $C^{18}OO$ and ~1/3 goes to $H_2^{18}O$.

Kinetic isotope fractionation between calcite and EIC (i.e., $\alpha_{c/EIC}$) is dependent on pH and growth rate, as described by the ion-by-ion model (Watkins et al., 2014) and a parameterized analytical expression (Devriendt et al., 2017b). Here, we adopt the ion-by-ion model of Watkins et al. (2014) but note that the Devriendt et al. (2017b) formulation produces nearly identical outputs at pH 8.3 and calcite growth rate = $10^{-6.3\ \pm\ 0.3}$ mol m^{-2} s^{-1}.

The free parameters of the model are F_{CO2} and F_{CaCO3}, and constraints on the functional form of each are discussed below.

4.2. $CaCO_3$ flux

The surface area normalized growth rate of $CaCO_3$ (moles m^{-2} s^{-1}) is dependent on the degree of supersaturation through a commonly used rate law (Nancollas and Reddy, 1971; Berner and Morse, 1974; Morse, 1978):

$$R = k(\Omega - 1)^n, \quad (15)$$

or in logarithmic form

$$\log_{10}R = \log_{10}k + n\log_{10}(\Omega - 1). \quad (16)$$

Zuddas and Mucci (1998) performed seeded calcite growth experiments using $CaCl_2$-NaCl solutions that closely match our solution compositions. Their data, which span a wide range of ionic strengths, are shown in Fig. 4. A linear regression using all of the Zuddas and Mucci (1998) data yields $n = 1.6$ and $k = 10^{-7.38}$. These values are used as a starting point, but the values can be adjusted to some degree, as permitted by the scatter of the data in Fig. 4.

The $CaCO_3$ flux is related to the growth rate through the relationship:

$$F_{\mathrm{CaCO_3}} = \mathrm{SA} \cdot R \quad (17)$$

where SA is the reactive surface area (m^2). At the onset of an unseeded experiment, SA = 0 and then it increases as calcite nucleates and grows. To calculate SA, we use a specific surface area, Sp, which is the surface area of calcite crystals at the end of an experiment (28 ± 5 m^2/mol for an average particle size of ~ 10 μm as determined from SEM images; Tang et al., 2008).

Using the model, we estimate that ~35% of the mass of crystals forms during the period of fast growth and ~65% forms during the period of steady-state growth. The growth rate values in Table 1 are based on the steady state growth rate and thus represent minimum estimates.

4.3. CO_2 flux

The flux of CO_2 (moles s^{-1}) into solution is expressed as

$$F_{\mathrm{CO_2}} = k_p\left([\mathrm{CO_2}]_{eq} - [\mathrm{CO_2}]\right) \quad (18)$$

where $[CO_2]_{eq}$ is calculated from Henry's constant and the pCO_2 of the gas tank (200 μatm in most experiments). The parameter k_p (kg-soln s^{-1}) describes the efficiency of gas transfer to solution, which varies between experiments depending on fluid dynamics (stirring) and the variable average bubble size produced by the diffusion stone. We therefore adjust k_p as needed to satisfy the constraint that the CO_2 influx matches the DIC outflux (i.e., the calcite growth rate) at steady state. For experiment S8, a value for $k_p = 0.0026$ kg-soln s^{-1} satisfies this constraint.

Table 3
Constants and parameters used in the model.

Symbol	Meaning	Value	Reference/Note
Part I: Model parameters			
V	Volume of solution (L)	1.7	-
F_{CO_2}	CO_2 flux into solution	$F_{CO_2} = mF_{CaCO_3} + b$	m and b to fit [DIC] data
R_{CaCO_3}	Carbonate precipitation rate (mol/m^2/s)	$R_{CaCO_3} = k(\Omega - 1)^n$ $n = 1.6$ $k = 10^{-7.38}$ $\Omega = \frac{[Ca^{2+}][CO_3^{2-}]}{K_{sp}}$	Zuddas and Mucci (1998)
Sp	Specific surface area (m^2/mol)	30	Tang et al. (2008)
SA	Total reactive surface area (m^2)	$Sp \cdot n_{CaCO3}$	-
F_{CaCO_3}	Carbonate precipitation flux (mol/s)	$SA \cdot R_{CaCO_3}$	-
Part II: Reaction rate constants			
χ	Fraction of HCO_3^- in EIC	$\chi = \left(1 + \frac{K_2}{[H^+]}\right)^{-1}$	K_2 from Millero et al. (2006)
k_{+1}	Rate const. CO_2 hydration (s^{-1})	$\log_{10}k_{+1} = 329.85 - 110.541\log_{10}(T_K) - \frac{17265.4}{T_K}$	Pinsent et al. (1956) and Uchikawa and Zeebe (2012)
k_{-1}	Rate const. CO_2 dehydration (M^{-1} s^{-1})	$k_{-1} = k_{+1}/K_1$	K_1 from Millero et al. (2007)
k_{+4}	Rate const. CO_2 hydrox. (M^{-1} s^{-1})	$\log_{10}k_{+4} = 13.635 - \frac{2895}{T_K}$	Pinsent et al. (1956) and Uchikawa and Zeebe (2012)
k_{-4}	Rate const. CO_2 dehydrox. (s^{-1})	$k_{-4} = k_{+4}\left(\frac{K_w}{K_1}\right)$	K_w from DOE (1994)
Part III: Isotopic parameters			
r_{CO_2}	$^{18}O/^{16}O$ ratio of CO_2	-	Isotope ratio
r_{EIC}	$^{18}O/^{16}O$ ratio of EIC	-	Isotope ratio
R_{CO_2}	$[C^{18}OO]/[CO_2]$	$2r_{CO_2}$	Isotopologue ratio
R_{EIC}	$[^{18}EIC]/[^{16}EIC]$	$3r_{EIC}$	Isotopologue ratio
$^{18}\chi$	Fraction of $HC^{18}OO_2^-$ in EIC	$^{18}\chi = \left(1 + \frac{K_2 \cdot \alpha_{CO_3^{2-}/HCO_3^-}}{[H^+]}\right)^{-1}$	K_2 from Millero et al. (2007)
a_{+1}, b_{+1}	Rate consts for hydration (s^{-1})	$a_{+1}/k_{+1} = 1.0000^{\dagger}$ $b_{+1}/k_{+1} = 0.9812^{\dagger}$	Yumol et al. (2020)
a_{-1}, b_{-1}	Rate consts for dehydration (M^{-1} s^{-1})	$a_{+1}/k_{+1} = K_1 \cdot \alpha_{HCO_3^-/H_2O}$ $b_{+1}/k_{+1} = K_1 \cdot \alpha_{HCO_3^-/CO_2}$	Equilibrium constraint Equilibrium constraint
a_{+4}, b_{+4}	Rate consts for hydrox. (M^{-1} s^{-1})	$a_{+4}/k_{+4} = 0.9988^{\ddagger}$ $b_{+4}/k_{+4} = 1.0000^{\ddagger}$	Christensen et al. (2021)
a_{-4}, b_{-4}	Rate consts for dehydrox. (s^{-1})	$\frac{a_{+4}}{k_{+4}} = \frac{K_1}{K_w} \cdot \frac{\alpha_{HCO_3^-/H_2O}}{\alpha_{OH^-/H_2O}}$ $b_{+4}/k_{+4} = \frac{K_1}{K_w} \cdot \alpha_{HCO_3^-/CO_2}$	Equilibrium constraint Equilibrium constraint
$\alpha_{c/EIC}$	Growth rate-dependent isotopic fractionation	$f(T, pH, [Ca^{2+}], [HCO_3^-], [CO_3^{2-}])$	Ion-by-ion model of Watkins et al. (2014)

† These values yield a bulk KFF that is consistent with Yumol et al. (2020).
‡ These values yield a bulk KFF that is consistent with Christensen et al. (2021).

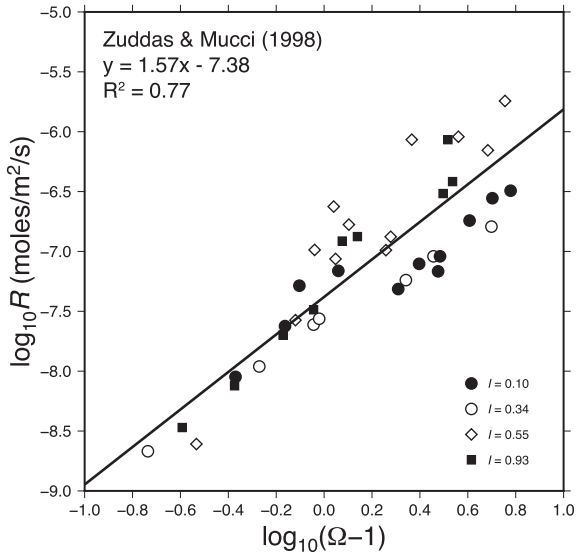

Fig. 4. Effect of the solution saturation (Ω) on calcite growth rate (R) in simple $CaCl_2$-NaCl solutions (data from Zuddas & Mucci, 1998). Seeded calcite precipitation experiments at varying ionic strength provide an empirical relationship between Ω and the surface area normalized growth rate R used in the model.

5. MODEL RESULTS

Model outputs are compared to data from two low salinity experiments (exp. S8 and CA4 with no NaCl) in Fig. 5. For the curves labeled "Model 1," the reactive surface area increases monotonically (Fig. 5a), which leads to a steadily decreasing [DIC] and Ω during Stage II. For the curves labeled "Model 2," the surface area of crystals is constant after the period of rapid nucleation and growth. This is akin to a seeded crystallization experiment where the reactive surface area is determined by the size distribution of seed crystals and assumed to be unchanging as overgrowth is added (e.g. Zuddas and Mucci, 1998). The different treatments of reactive surface area between Models 1 and 2 have little effect on the resulting isotopic composition of calcite.

The F_{CO2} and F_{CaCO3} curves (Fig. 5b and c) illustrate the negative feedback that leads to steady state behavior. The flux of CO_2 is at a maximum value initially because $[CO_2(aq)] \sim 0$ and it decreases steadily during Stage I as $[CO_2(aq)]$ accumulates in solution (Eq. (18)). The accumulation of $[CO_2(aq)]$ leads to an increase in F_{CaCO3} into Stage II. This acts to draw down the $[CO_2(aq)]$, which is then compensated by an increase in F_{CO2} at the beginning of Stage II. A few hours into Stage II, F_{CaCO3} and F_{CO2} are nearly in balance. The model k_p parameter that yields a match to the steady state growth rate (Fig. 5c) also matches the evolution of [DIC] (Fig. 5d), suggesting that the rate law derived from the seeded experiments of Zuddas and Mucci (1998) is valid for our unseeded experiments.

In the absence of bCA enzyme (i.e. uncatalyzed experiment), the $1000\ln\alpha$ of $CO_{2(aq)}$ begins at the equilibrium value and then steeply drops (Fig. 5e) because of the input of bubbled $CO_{2(g)}$ with $\delta^{18}O \sim 24.3‰$ VSMOW ($\sim 5‰$ lower than the equilibrium value). The light CO_2 undergoes hydration and hydroxylation to form isotopically light EIC initially (Fig. 5f), but as the DIC residence time in solution increases due to increasing [DIC], the CO_2 hydration reaction becomes increasingly bi-directional ($R_b/R_f \rightarrow 1$, where R_b is the backward rate and R_f is the forward rate; Fig. 5g), leading to a progressively isotopically heavier EIC pool during Stage I that approaches the EIC equilibrium value. Around the 21-hour mark, the $CaCO_3$ flux is sufficiently high, leading to higher R_f/R_b for the hydration reaction and isotopically lighter EIC pool until steady state is reached during Stage II. Without any enzyme added, the time-integrated $1000\ln\alpha_{c/w}$ values are 25.3 for Model 1 and 25.6 for Model 2, which agree well with the measured 25.3 value.

With a [bCA] of 0.2 μM, the rate constant of CO_2 hydration (k_{+1}) is increased by a factor of 200 (Uchikawa and Zeebe, 2012) and the $1000\ln\alpha_{EIC/w}$ is equilibrated for all but the first couple hours of the simulated experiments (Fig. 5f). The $1000\ln\alpha_{c/w}$ values are 28.0 for Model 1 and 27.9 for Model 2 (Fig. 5h), which match the measured value of 28.0 and is ~1.5–2‰ lower than the equilibrium value due to the growth rate-dependent calcite-CO_3^{2-} and calcite-HCO_3^- fractionation.

6. DISCUSSION

6.1. The effect of ionic strength on the oxygen isotope fractionation between calcite and the EIC

Mineral-anion KFFs may be dependent on solution composition. The kinetics of calcite growth and dissolution have been postulated to depend NaCl concentration (Zuddas and Mucci, 1998). Hence it could be expected that ionic strength affects the calcite dissolution/precipitation ratio and by extension the isotopic fractionation between calcite and CO_3^{2-} (and HCO_3^-) (Devriendt et al., 2017b). The observation that the maximum measured $1000\ln\alpha_{c/w}$ for a given [NaCl] does not vary up to [NaCl] of 0.35 M suggests that the calcite-CO_3^{2-} (and possibly calcite-HCO_3^-) KFF(s) is/are independent of change in ionic strength caused by Na^+ and Cl^- ions, contrary to the hypothesis proposed by Devriendt et al. (2017b). The decrease in the maximum $1000\ln\alpha_{c/w}$ above [NaCl] = 0.35 M could be attributed to a changing calcite-EIC KFF but that would require an abrupt change in crystal growth mechanism or surface speciation for which there is no independent evidence.

6.2. The origin of $\delta^{18}O_{calcite}$ variability at high ionic strength

Experiments with [NaCl] > 0.35 M display lower and more variable $1000\ln\alpha_{c/w}$ values despite the very high [bCA] (up to 3 μM) used in these experiments. In the following subsections, we consider the possible explanations for this variability, including the $\delta^{18}O$ of free water, the effect of ion pairs, the effect of NaCl on DIC speciation, and the effect of dissolved salts on the enzyme kinetics.

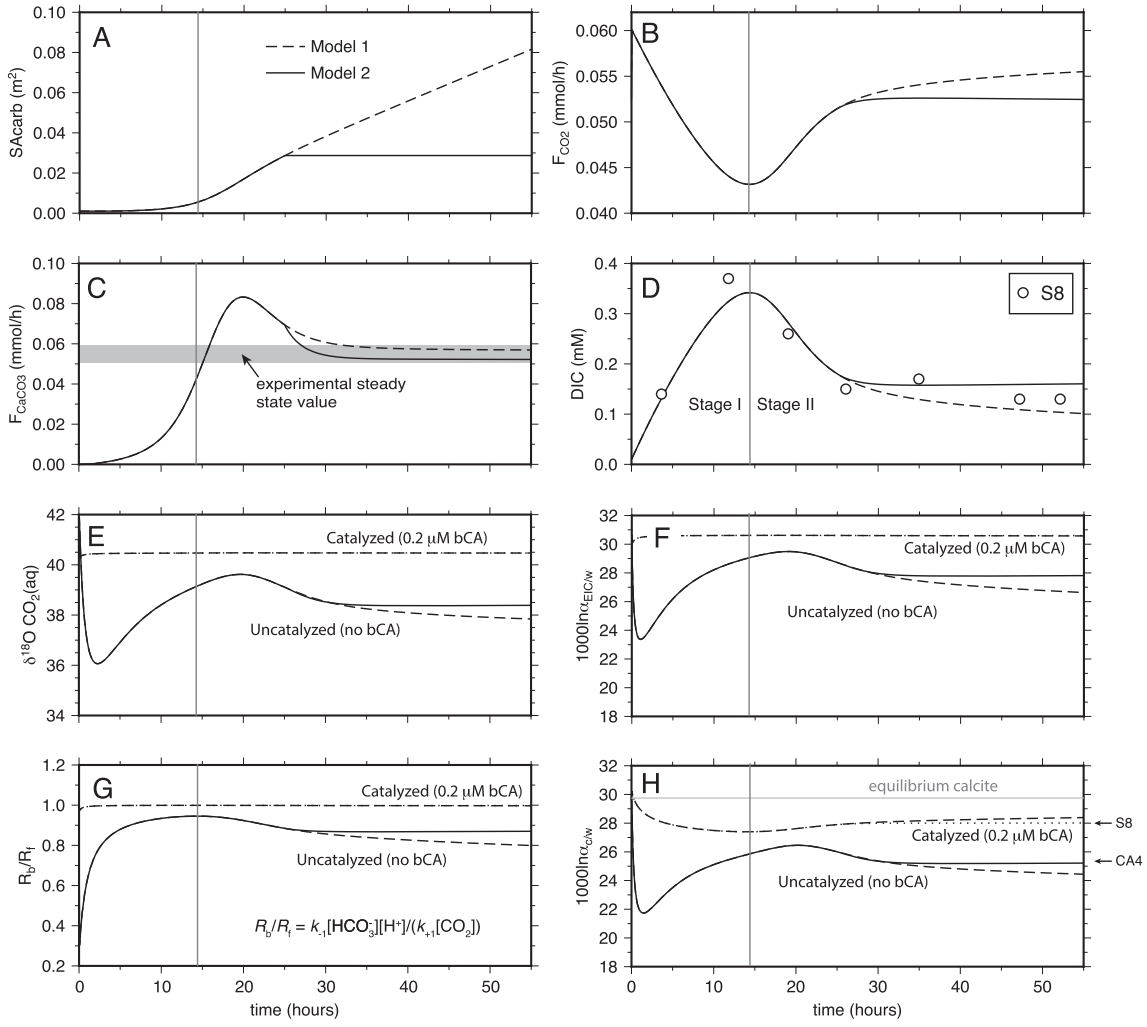

Fig. 5. Model for the time-dependent behavior in experiments S8 and CA4 at $T = 25$ °C, pH = 8.3 and [NaCl] = 0 M. Model 1 assumes that the reactive surface area of carbonate crystals is proportional to the mass of carbonate precipitated whereas Model 2 treats the steady state portion of Stage II as a seeded experiment with fixed reactive surface area. The two different approaches yield similar isotopic outputs and are in good agreement with measured $1000\ln\alpha_{c/w}$ values.

6.2.1. Effect of dissolved ions on $\delta^{18}O_w$

Isotopically heavy oxygen is concentrated in the hydration spheres of some cations or anions in solution, resulting in an oxygen isotope composition of free water that is potentially lighter than the $\delta^{18}O$ of the overall solution (Taube, 1954). However, the hydration spheres of Na^+ and Cl^- do not fractionate oxygen isotopes, regardless of solution molality (Taube, 1954). The other cations in our solutions exhibit opposing behavior, with Ca^{2+} ions having isotopically heavy hydration spheres (Sofer and Gat, 1972) and NH_4^+ ions having isotopically light hydration spheres (Taube, 1954). Although we use Ca^{2+} and NH_4^+, our solutions are far too dilute with respect to these ions to expect a resolvable effect. A salt effect on hydration spheres is therefore not responsible for the $1000\ln\alpha_{c/w}$ variations.

6.2.2. Effect of ion pairing on oxygen isotope fractionation between DIC species and H_2O

The equilibrium fractionation factors in the CO_2-H_2O system ($\alpha_{CO_2\text{-}H_2O}$, $\alpha_{HCO_3^-\text{-}H_2O}$ and $\alpha_{CO_3^{2-}\text{-}H_2O}$) are based on freshwater solutions (Beck et al., 2005). The addition of dissolved salts can lead to significant fractions of bicarbonate and carbonate ions existing as cation-CO_3^{2-} complexes such as $NaHCO_3^0$ and $NaCO_3^-$, which may shift the isotopic composition of the HCO_3^- and CO_3^{2-} compounds reacting with Ca^{2+} to form $CaCO_3$. Kim et al. (2014) showed that variable amounts of dissolved NaCl ($I = 0$–0.7) have a negligible effect on the equilibrium fractionation factors in the Na-Cl-CO_2-H_2O system. Similarly, Uchikawa and Zeebe (2013) found no discernible effects of $MgCO_3^0$ on oxygen isotope equilibrium in the Mg-Cl-CO_2-H_2O system over a

large range of $MgCO_3^0$ abundances (0 to 40% of total CO_3^{2-}). Hence, isotope partitioning among ion pairs is not responsible for the $1000\ln\alpha_{c/w}$ variations.

6.2.3. Effect of DIC speciation on $\delta^{18}O_{calcite}$

The relative proportions of CO_3^{2-} and HCO_3^- within the EIC may affect $\delta^{18}O_{calcite}$ where HCO_3^- attachment to the calcite surface is significant (Wolthers et al., 2012; Watkins et al., 2014). This is because CO_3^{2-} and HCO_3^- have distinct oxygen isotope compositions (Fig. 3; Beck et al., 2005). Increasing salinity shifts the solution to higher CO_3^{2-}/DIC (e.g. Millero et al., 2007), which decreases the $\delta^{18}O$ of the EIC. Moreover, the DIC equilibration time increases at higher CO_3^{2-}/DIC due to lower $[CO_2]$ (Usdowski et al., 1991; Uchikawa and Zeebe, 2012).

In simple NaCl solutions, the CO_3^{2-}/DIC ratio increases from 1.8% to 5.3% between [NaCl] = 0 and 0.5 M, with very little change above [NaCl] = 0.5 M (Millero et al., 2007, Fig. S1.1e). However, this increase in CO_3^{2-}/DIC only lowers the $\delta^{18}O$ of isotopically equilibrated DIC by about 0.3‰ (Fig. 3). In addition, the change in speciation translates to a minor increase in the DIC equilibration time that is accounted for in our model. Hence, a salt effect on solution speciation and equilibration time is not responsible for the $1000\ln\alpha_{c/w}$ variations.

6.2.4. Effect of NaCl on the kinetics of catalyzed CO_2 (de) hydration

The enzyme bCA increases the CO_2 (de)hydration rate constants k_{+1} and k_{-1}. According to the Michaelis-Menten kinetic model, the expression for the enzyme-catalyzed rate constant for CO_2 hydration is:

$$k_{+1}{}^* = k_{+1} + \frac{k_{cat}}{K_M} \cdot [CA], \tag{19}$$

where k_{cat} is the turnover number and K_M is the Michaelis-Menten constant. Uchikawa and Zeebe (2012) determined $k_{cat}/K_M = 2.7 \times 10^7\ M^{-1}\ s^{-1}$ for bCA in NaCl-free solutions. In the absence of an inhibitor, addition of 0.2 μM bCA is expected to increase k_{+1} by a factor of 200 in freshwater solutions.

Many inorganic and organic compounds are known to inhibit the activity of various forms of carbonic anhydrase (Bertucci et al., 2009, 2011a; De Simone and Supuran, 2012; Del Prete et al., 2014). Previous studies have found that several anions (including Cl^-, Br^-, and NO_3^-) affect the activity of CA. Nielsen and Frieden (1972) found these anions to have an inhibitory effect on the activity of both oyster CA and bovine CA, while Dionisio-Sese and Miyachi (1992) studied a variety of marine algae and found that the inhibitory or catalytic effects of these anions on CA activity was species-dependent, with a proposed mechanism for inhibition being that these anions may displace the hydroxyl group bound to the zinc at the enzyme active site. Enzyme inhibition is typically expressed in terms of an inhibition constant, K_I (mM), which is the concentration of inhibitor at which the rate of the uninhibited reaction is reduced by a factor of 2. The larger the value of K_I, the weaker the inhibitor.

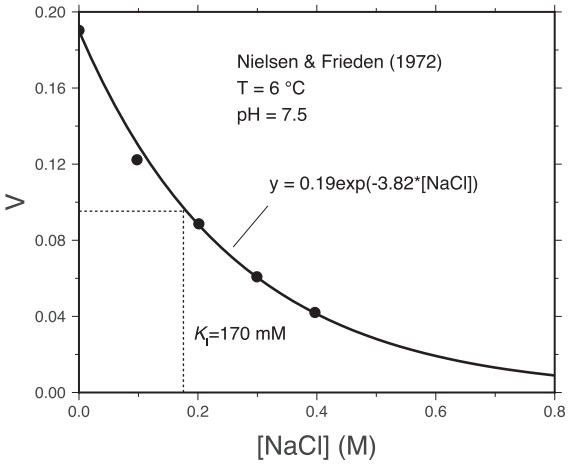

Fig. 6. The pH-stat assays of Nielsen and Frieden (1972) conducted at pH 7.5 and a temperature of 6 °C suggest an exponential dependence of CO_2 (de)hydration reaction velocity (V) on [NaCl]. The data gives an exponent of −3.82 and an inhibition constant K_I = 170 mM.

Nielsen and Frieden (1972) carried out pH-stat assays and reported K_I = 170 mM for bCA at T = 6 °C and pH = 7.5. They showed the CO_2 (de)hydration reaction velocity (V) decreases exponentially with increasing [NaCl] (Fig. 6). They define V as the difference between the catalyzed versus uncatalyzed reaction velocity, which in turn, we infer to be directly proportional to k_{cat}/K_M. Their results can be used to write an equation for k_{cat}/K_M that depends explicitly on [NaCl]:

$$\frac{k_{cat}}{K_M} = \left(\frac{k_{cat}}{K_M}\right)_{[NaCl=0]} \exp(A \cdot [NaCl]), \tag{20}$$

where the exponent A describes the strength of inhibition. Our fit to the data from Nielsen and Frieden (1972) gives A = −3.82 (Fig. 6).

To assess whether NaCl as a mild inhibitor can account for our observations, Fig. 7 shows model outputs using the functional form for k_{cat}/K_M from Eq. (20). Model outputs are obtained using the same parameters from experiment S8 and CA4 (Fig. 5) but with k_{+1}* (Eqs. (19) and (20)) instead of k_{+1} in reactions (4), (6) and (8), and by varying [bCA] and [NaCl]. Model results using A = −3.82 (K_I = 170 mM, based on data from Nielsen and Frieden, 1972) are shown on the left panels of Fig. 7 (panels a to d). Measured data and model outputs are compared in two separate panels (Fig. 7b and c) because the $\delta^{18}O$ of DIC species under non-equilibrium conditions depends on the $\delta^{18}O$ of bubbled CO_2 (Supplement S2): (1) experiments with high $\delta^{18}O_{CO2(g)}$ (22.2–24.3‰, Fig. 7b) and (2) experiments with low $\delta^{18}O_{CO2(g)}$ (12.27–13.45‰, Fig. 7c). Model outputs shown in Fig. 7b and 7c involve no free parameters and yet can explain several first-order features of the dataset: (1) The range of measured $1000\ln\alpha_{c/w}$ values in the high $\delta^{18}O_{CO2(g)}$ experiments is about 3‰. (2) About 1 μM bCA is required to maintain an isotopically equilibrated DIC pool up to [NaCl] ~ 0.35 M. (3) Maintaining DIC at isotopic equilibrium with bCA becomes increasingly difficult

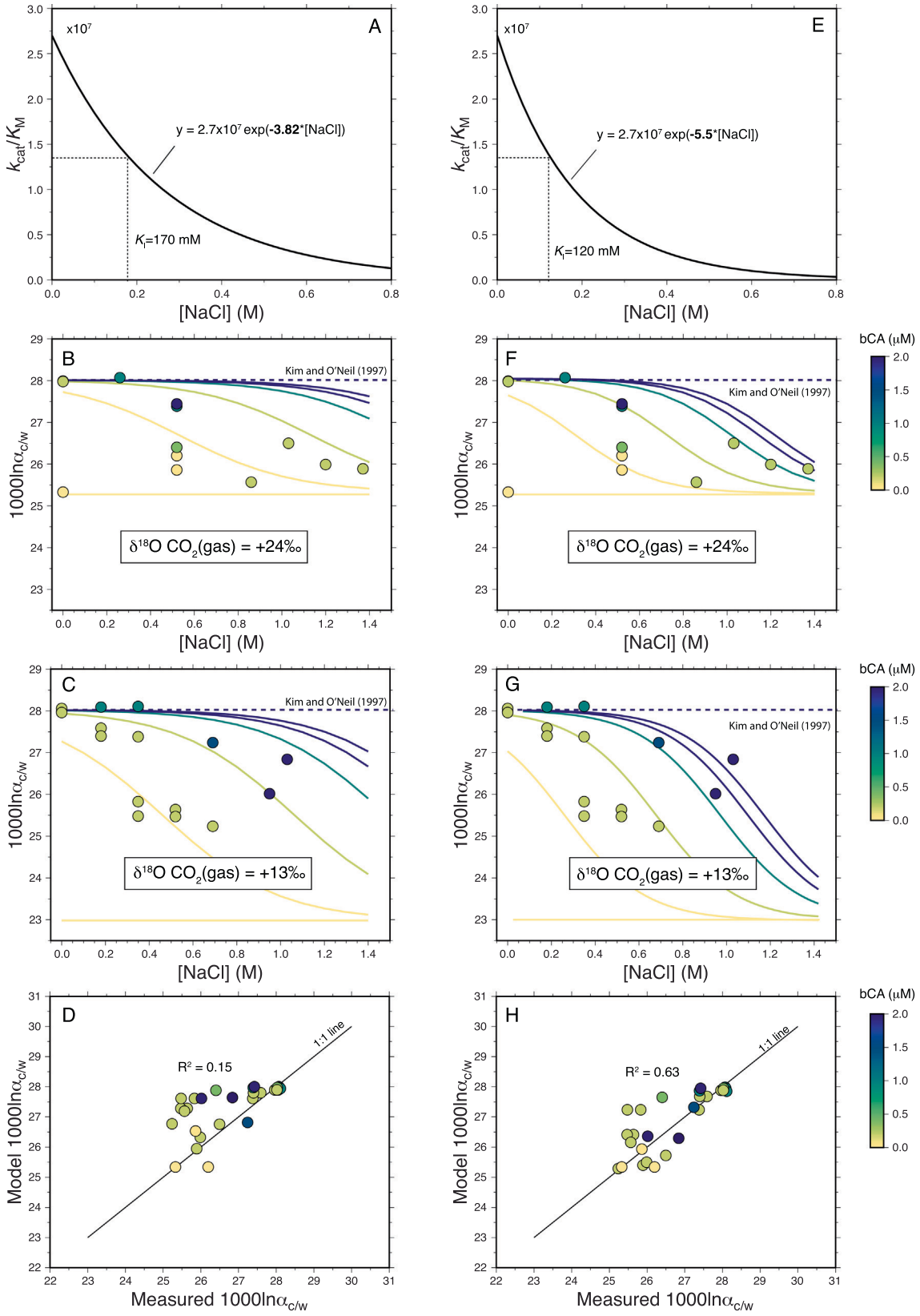

Fig. 7. Data-model comparison for the calcite-water oxygen isotope fractionation ($1000\ln\alpha_{c/w}$) in solutions with different NaCl concentrations (0–1.4 M). Model outputs were obtained using Eqs. (19) and (20) for the NaCl dependence of the catalyzed CO_2 (de)hydroxylation reaction kinetic (as in Fig. 6). Left panels (A–D) show results using an exponent of −3.82 (Nielsen and Frieden, 1972). Right panels (E-H) show results using an exponent of −5.5. For panels (B) and (F), the input gas has high $\delta^{18}O$ (22.2–24.3‰). For panels (C) and (G), the input gas has low $\delta^{18}O$ (12.27–13.45‰). The NaCl dependence of Nielsen and Frieden (1972) is weaker than indicated by our experiments, leading to model $1000\ln\alpha_{c/w}$ values that are systematically higher (i.e., more equilibrated DIC) than the measured values (panel D). A stronger inhibition by NaCl yields better overall agreement between model and data (panel H).

above [NaCl] = 0.35 M even with 2–3 μM of bCA added. (4) There is a general decrease, for a given [bCA], in the $1000\ln\alpha_{c/w}$ values with increasing [NaCl]. However, the model $1000\ln\alpha_{c/w}$ values are systematically higher than the measured values for all experiments with bCA, implying that the modeled NaCl inhibition is too weak and that the modeled DIC pool is more equilibrated than suggested by the data (Fig. 7d).

The data-model agreement is improved using A = −5.5 (K_I = 120 mM, Fig. 7e–h). There are a couple of possible reasons why the inhibitory effect of NaCl on bCA may be stronger in our experiments than suggested by the data of Nielsen and Frieden (1972). First, the Nielsen and Frieden (1972) parameters were derived from a solution with a lower temperature and pH than our experiments and it is conceivable that NaCl inhibition varies with either or both of these parameters. Second, it is possible that they used a different isozyme of bCA, and different isozymes can have substantially different K_I values (De Simone and Supuran, 2012).

Overall, these results suggest that the most up-to-date values for the kinetic fractionation factors (Table 3) and functional form of the salt effect on bCA from Nielsen and Frieden (1972) are an accurate quantitative description of our calcite growth experiments and should be useful for modeling the $\delta^{18}O$ of $CaCO_3$ in other experiments and natural environments.

7. IMPLICATIONS

7.1. Towards a general model for kinetic oxygen isotope effects

The current work builds on a large number of studies, each contributing to the development of a general model of kinetic oxygen isotope fractionation in the $CaCO_3$-DIC-H_2O system (e.g. Clark et al., 1992; Usdowski and Hoefs, 1993; Zeebe and Wolf-Gladrow, 2001; Beck et al., 2005; Kim et al., 2006; DePaolo, 2011; Nielsen et al., 2012; Watkins et al., 2013, 2014, 2017; Zeebe, 2014; Devriendt et al., 2017b; Sade and Halevy, 2017; Chen et al., 2018; Yumol et al., 2020; Zeebe, 2020; Guo and Zhou, 2019; Guo, 2020; Christensen et al., 2021). This study presents the first attempt to model kinetic oxygen isotope effects recorded in laboratory grown calcite with a fully reversible isotopic box model (Chen et al., 2018; Christensen et al., 2021) and provides a functional form for the inhibitory effect of NaCl on the catalytic effect of bovine carbonic anhydrase. The success of the model applied to our experiments with variably equilibrated DIC pools (Fig. 7f–h) suggests that the community is converging towards an accurate set of equilibrium and kinetic fractionation factors in the $CaCO_3$-DIC-H_2O system that will be useful for improving models of isotopic disequilibrium and biological 'vital effects' in other settings.

7.2. Application to marine calcifiers

Carbonic anhydrase (CA) is present at or near the site of calcification of many (if not all) biological organisms, including urchins (e.g. Mitsunaga et al., 1986), crustaceans (e.g. Henry, 2001), corals (e.g. Furla et al., 2000; Moya et al., 2008; Tambutté et al., 2011; Bertucci et al., 2011b; Mass et al., 2014), coccolithophores (e.g. Zhang et al., 2021), and foraminifera (e.g. de Goeyse et al., 2021). Despite the presence of CA, all of these organisms produce $CaCO_3$ skeletons or tests that exhibit deviations from isotopic equilibrium (e.g., McConnaughey, 1989; Spero et al., 1997; Adkins et al., 2003; Kimball et al., 2014; Hermoso et al., 2014; Devriendt et al., 2017a; Chen et al., 2018).

The pervasiveness of KIEs in the marine carbonate record has motivated efforts to develop isotopic biomineralization models. Recent approaches for coral and coccolith calcification invoke a CO_2-fed fluid and explicitly account for carbonic anhydrase activity on KIEs in the DIC-water system (Devriendt et al., 2017b; Chen et al., 2018; Zhang et al., 2021). For both organisms, the parameter k_{cat}/K_M has been treated as a constant. Given that the composition of the calcifying fluid is likely to have higher pH and lower salinity than ambient seawater due to proton pumping and cation selectivity, respectively, the treatment of constant k_{cat}/K_M may warrant relaxation in future refinements. An obvious caveat is that the bCA used herein may not be representative of CA found in marine organisms. For example, it is possible that marine varieties of CA are less sensitive to salt inhibition, either through modifications to the enzyme structure or by screening inhibitors from the calcifying fluid (e.g. Dionisio-Sese and Miyachi, 1992; Bertucci et al., 2009).

8. SUMMARY

Calcite crystals were precipitated at 25 °C in solutions of variable NaCl and bovine carbonic anhydrase (bCA) concentrations to investigate the effect of a solution ionic strength on the oxygen isotope fractionation between calcite and an isotopically equilibrated DIC pool (EIC). The experimental results indicate no significant ionic strength effects on calcite-EIC oxygen isotope fractionation but revealed the inhibitory effect of NaCl on the catalyzed CO_2 (de)hydration reaction. This led to DIC pools that were not isotopically equilibrated and variable $1000\ln\alpha_{c/w}$ values in high ionic strength solutions ([NaCl] > 0.35 M). Using an updated isotopic box model and accurate measurements of solution parameters ([TA], [DIC] and $\delta^{18}O$ of input $CO_{2(g)}$), we successfully modeled the measured variability in $1000\ln\alpha_{c/w}$ values at high [NaCl] and quantified the inhibitory effect of NaCl on bCA. The new parameterization of the dependence of bCA activity on [NaCl] can be used in biochemical models of calcification with the caveat that other isozymes of CA may be less sensitive to inhibition by dissolved salts and solution pH. This is a sub-

ject that warrants further investigation for understanding vital effects in biogenic calcite and for finding an alternative to bCA for equilibrating the DIC pool in experiments that involve seawater-like compositions.

Declaration of Competing Interest

The authors declare that they have no known competing financial interests or personal relationships that could have appeared to influence the work reported in this paper.

ACKNOWLEDGEMENTS

We are grateful for help from Andrew Ross, Jennifer McKay (OSU CEOAS Stable Isotope Laboratory) and James Palandri (UO Stable Isotope Laboratory) for isotope analyses. This paper benefited from the comments of Joji Uchikawa and two anonymous reviewers. This research was supported by NSF grant no. EAR1749183 to JMW.

APPENDIX A. SUPPLEMENTARY MATERIAL

Supplementary data to this article can be found online at https://doi.org/10.1016/j.gca.2022.01.028.

REFERENCES

Adkins J. F., Boyle E. A., Curry W. B. and Lutringer A. (2003) Stable isotopes in deep-sea corals and a new mechanism for "vital effects". *Geochim. Cosmochim. Acta* **67**, 1129–1143.

Baker E. B. (2015) *Carbon and Oxygen Isotope Fractionation in Laboratory-Precipitated, Inorganic Calcite*. University of Oregon.

Beck W. C., Grossman E. L. and Morse J. W. (2005) Experimental studies of oxygen isotope fractionation in the carbonic acid system at 15°, 25°, and 40°C. *Geochim. Cosmochim. Acta* **69**, 3493–3503.

Berner R. A. and Morse J. W. (1974) Dissolution Kinetics of Calcium Carbonate in Sea Water IV. Theory of Calcite Dissolution. *Am. J. Sci.* **274**, 108–134.

Bertucci A., Innocenti A., Zoccola D., Scozzafava A., Allemand D., Tambutté S. and Supuran C. T. (2009) Carbonic anhydrase inhibitors: Inhibition studies of a coral secretory isoform with inorganic anions. *Bioorganic Med. Chem. Lett.* **19**, 650–653.

Bertucci A., Innocenti A., Scozzafava A., Tambutté S., Zoccola D. and Supuran C. T. (2011a) Carbonic anhydrase inhibitors. Inhibition studies with anions and sulfonamides of a new cytosolic enzyme from the scleractinian coral Stylophora pistillata. *Bioorganic Med. Chem. Lett.* **21**, 710–714.

Bertucci A., Tambutté S., Supuran C. T., Allemand D. and Zoccola D. (2011b) A New Coral Carbonic Anhydrase in Stylophora pistillata. *Mar. Biotechnol.* **13**, 992–1002.

Bigeleisen J. and Mayer M. G. (1947) Calculation of Equilibrium Constants for Isotopic Exchange Reactions. *J. Chem. Phys.* **15**, 261–267.

Brenninkmeijer C. A. M., Kraft P. and Mook W. G. (1983) Oxygen isotope fractionation between CO_2 and H_2O. *Chem. Geol.* **41**, 181–190.

Charlton S. R. and Parkhurst D. L. (2011) Modules based on the geochemical model PHREEQC for use in scripting and programming languages. *Comput. Geosci.* **37**, 1653–1663.

Chen S., Gagnon A. C. and Adkins J. F. (2018) Carbonic anhydrase, coral calcification and a new model of stable isotope vital effects. *Geochim. Cosmochim. Acta* **236**, 179–197.

Christensen J. N., Watkins J. M., Devriendt L. S., DePaolo D. J., Conrad M. E., Voltolini M., Yang W. and Dong W. (2021) Isotopic fractionation accompanying CO_2 hydroxylation and carbonate precipitation from high pH waters at The Cedars, California, USA. *Geochim. Cosmochim. Acta* **301**, 91–115.

Clark I. D., Fontes J. C. and Fritz P. (1992) Stable isotope disequilibria in travertine from high pH waters: Laboratory investigations and field observations from Oman. *Geochim. Cosmochim. Acta* **56**, 2041–2050.

Coplen T. B. (2007) Calibration of the calcite-water oxygen-isotope geothermometer at Devils Hole, Nevada, a natural laboratory. *Geochim. Cosmochim. Acta* **71**, 3948–3957.

Coplen T. B., Kendall C. and Hopple J. (1983) Comparison of stable isotope reference samples. *Nature* **302**, 236–238.

De Goeyse S., Webb A. E., Reichart G.-J. and De Nooijer L. J. (2021) Carbonic anhydrase is involved in calcification by the benthic foraminifer Amphistegina lessonii. *Biogeosciences* **18**, 393–401.

De Lucia M. and Kühn M. (2013) Coupling R and PHREEQC: efficient programming of geochemical models. *Energy Proc.* **40**, 464–471.

De Simone G. and Supuran C. T. (2012) (In)organic anions as carbonic anhydrase inhibitors. *J. Inorg. Biochem.* **111**, 117–129.

Del Prete S., Vullo D., Scozzafava A., Capasso C. and Supuran C. T. (2014) Cloning, characterization and anion inhibition study of the δ-class carbonic anhydrase (TweCA) from the marine diatom Thalassiosira weissflogii. *Bioorganic Med. Chem.* **22**, 531–537.

DePaolo D. J. (2011) Surface kinetic model for isotopic and trace element fractionation during precipitation of calcite from aqueous solutions. *Geochim. Cosmochim. Acta* **75**, 1039–1056.

Devriendt L. S., McGregor H. V. and Chivas A. R. (2017a) Ostracod calcite records the $^{18}O/^{16}O$ ratio of the bicarbonate and carbonate ions in water. *Geochim. Cosmochim. Acta* **214**, 30–50.

Devriendt L. S., Watkins J. M. and McGregor H. V. (2017b) Oxygen isotope fractionation in the $CaCO_3$-DIC-H_2O system. *Geochim. Cosmochim. Acta* **214**, 115–142.

Dionisio-Sese M. L. and Miyachi S. (1992) The Effect of Sodium Chloride on Carbonic Anhydrase Activity in Marine Microalgae. *J. Phycol.* **28**, 619–624.

DOE (1994) Handbook of Methods for the Analysis of the Various Parameters of the Carbon Dioxide System in Sea water. Version 2 (eds. A. G. Dickson and C. Goyet), ORNL/CDIAC-74, Oak Ridge, Tennessee.

Furla P., Allemand D. and Orsenigo M. N. (2000) Involvement of H^+-ATPase and carbonic anhydrase in inorganic carbon uptake for endosymbiont photosynthesis. *Am. J. Physiol. - Regul. Integr. Comp. Physiol.* **278**, R870–R881.

Guo W. (2020) Kinetic clumped isotope fractionation in the DIC-H_2O-CO_2 system: Patterns, controls, and implications. *Geochim. Cosmochim. Acta* **268**, 230–257.

Guo W. and Zhou C. (2019) Triple oxygen isotope fractionation in the DIC-H_2O-CO_2 system: A numerical framework and its implications. *Geochim. Cosmochim. Acta* **246**, 541–564.

Henry R. P. (2001) Environmentally mediated carbonic anhydrase induction in the gills of euryhaline crustaceans. *J. Exp. Biol.* **204**, 991–1002.

Hermoso M., Horner T. J., Minoletti F. and Rickaby R. E. M. (2014) Constraints on the vital effect in coccolithophore and dinoflagellate calcite by oxygen isotopic modification of seawater. *Geochim. Cosmochim. Acta* **141**, 612–627.

Hong M. and Teng H. H. (2014) Implications of solution chemistry effects: Direction-specific restraints on the step kinetics of calcite growth. *Geochim. Cosmochim. Acta* **141**, 228–239.

Jacobson R. L. and Langmuir D. (1974) Dissociation constants of calcite and $CaHCO_3^+$ from 0 to 50°C. *Geochim. Cosmochim. Acta* **38**, 301–318.

Kim S.-T. and O'Neil J. R. (1997) Equilibrium and nonequilibrium oxygen isotope effects in synthetic carbonates. *Geochim. Cosmochim. Acta* **61**, 3461–3475.

Kim S.-T., Hillaire-Marcel C. and Mucci A. (2006) Mechanisms of equilibrium and kinetic oxygen isotope effects in synthetic aragonite at 25 °C. *Geochim. Cosmochim. Acta* **70**, 5790–5801.

Kim S.-T., Gebbinck C. K., Mucci A. and Coplen T. B. (2014) Oxygen isotope systematics in the aragonite–CO_2–H_2O–NaCl system up to 0.7 mol/kg ionic strength at 25 °C. *Geochim. Cosmochim. Acta* **137**, 147–158.

Kimball J. B., Dunbar R. B. and Guilderson T. P. (2014) Oxygen and carbon isotope fractionation in calcitic deep-sea corals: Implications for paleotemperature reconstruction. *Chem. Geol.* **381**, 223–233.

Mass T., Drake J. L., Peters E. C., Jiang W. and Falkowski P. G. (2014) Immunolocalization of skeletal matrix proteins in tissue and mineral of the coral Stylophora pistillata. *Proc. Natl. Acad. Sci. USA* **111**, 12728–12733.

McConnaughey T. (1989) ^{13}C and ^{18}O isotopic disequilibrium in biological carbonates: I. Patterns. *Geochim. Cosmochim. Acta* **53**, 151–162.

Millero F. J., Graham T. B., Huang F., Bustos-Serrano H. and Pierrot D. (2006) Dissociation constants of carbonic acid in seawater as a function of salinity and temperature. *Mar. Chem.* **100**, 80–94.

Millero F., Huang F., Graham T. and Pierrot D. (2007) The dissociation of carbonic acid in NaCl solutions as a function of concentration and temperature. *Geochim. Cosmochim. Acta* **71**, 46–55.

Mitsunaga K., Akasaka K., Shimada H., Fujino Y., Yasumasu I. and Numanoi H. (1986) Carbonic anhydrase activity in developing sea urchin embryos with special reference to calcification of spicules. *Cell Differ.* **18**, 257–262.

Morse J. W. (1978) Dissolution kinetics of calcium carbonate in sea water: VI. The near-equilibrium dissolution kinetics of calcium carbonate-rich deep sea sediments. *Am. J. Sci.* **278**, 344–353.

Moya A., Tambutté S., Bertucci A., Tambutté E., Lotto S., Vullo D., Supuran C. T., Allemand D. and Zoccola D. (2008) Carbonic anhydrase in the scleractinian coral Stylophora pistillata: Characterization, localization, and role in biomineralization. *J. Biol. Chem.* **283**, 25475–25484.

Mucci A. (1983) The solubility of calcite and aragonite in seawater at various salinities, temperatures, and one atmosphere total pressure. *Am. J. Sci.* **283**, 780–799.

Nancollas G. H. and Reddy M. M. (1971) The crystallization of calcium carbonate. II. Calcite growth mechanism. *J. Colloid Interface Sci.* **37**, 824–830.

Nielsen L. C., DePaolo D. J. and De Yoreo J. J. (2012) Self-consistent ion-by-ion growth model for kinetic isotopic fractionation during calcite precipitation. *Geochim. Cosmochim. Acta* **86**, 166–181.

Nielsen S. A. and Frieden E. (1972) Some chemical and kinetic properties of oyster carbonic anhydrase. *Comp. Biochem. Physiol. Part B Comp. Biochem.* **41**, 875–889.

O'Leary M. H. (1984) Measurement of the isotope fractionation associated with diffusion of carbon dioxide in aqueous solution. *J. Phys. Chem.* **88**, 823–825.

Pinsent B. R. W., Pearson L. and Roughton F. J. W. (1956) The kinetics of combination of carbon dioxide with ammonia. *Trans. Faraday Soc.* **52**, 1594–1598.

Ruiz-Agudo E., Kowacz M., Putnis C. V. and Putnis A. (2010) The role of background electrolytes on the kinetics and mechanism of calcite dissolution. *Geochim. Cosmochim. Acta* **74**, 1256–1267.

Ruiz-Agudo E., Putnis C. V., Wang L. and Putnis A. (2011) Specific effects of background electrolytes on the kinetics of step propagation during calcite growth. *Geochim. Cosmochim. Acta* **75**, 3803–3814.

Sade Z. and Halevy I. (2017) New constraints on kinetic isotope effects during $CO_{2(aq)}$ hydration and hydroxylation: Revisiting theoretical and experimental data. *Geochim. Cosmochim. Acta* **214**, 246–265.

Sofer Z. and Gat J. R. (1972) Activities and Concentrations of Oxygen-18 in Concentrated Aqueous Salt Solutions: Analytical and Geophysical Implications. *Earth Planet. Sci. Lett.* **15**, 232–238.

Spero H. J., Bijma J., Lea D. W. and Bernis B. E. (1997) Effect of seawater carbonate concentration on foraminiferal carbon and oxygen isotopes. *Nature* **390**, 497–500.

Tambutté S., Holcomb M., Ferrier-Pagès C., Reynaud S., Tambutté É., Zoccola D. and Allemand D. (2011) Coral biomineralization: From the gene to the environment. *J. Exp. Mar. Bio. Ecol.* **408**, 58–78.

Tang J., Köhler S. J. and Dietzel M. (2008) Sr^{2+}/Ca^{2+} and $^{44}Ca/^{40}Ca$ fractionation during inorganic calcite formation: I. Sr incorporation. *Geochim. Cosmochim. Acta* **72**, 3718–3732.

Taube H. (1954) Use of Oxygen Isotope Effects in the Study of Hydration of Ions. *J. Phys. Chem.* **58**, 523–528.

Uchikawa J. and Zeebe R. E. (2012) The effect of carbonic anhydrase on the kinetics and equilibrium of the oxygen isotope exchange in the CO_2-H_2O system: Implications for $\delta^{18}O$ vital effects in biogenic carbonates. *Geochim. Cosmochim. Acta* **95**, 15–34.

Uchikawa J. and Zeebe R. E. (2013) No discernible effect of Mg^{2+} ions on the equilibrium oxygen isotope fractionation in the CO_2-H_2O system. *Chem. Geol.* **343**, 1–11.

Uchikawa J., Chen S., Eiler J. M., Adkins J. F. and Zeebe R. E. (2021) Trajectory and timescale of oxygen and clumped isotope equilibration in the dissolved carbonate system under normal and enzymatically-catalyzed conditions at 25 °C. *Geochim. Cosmochim. Acta* **314**, 313–333.

Urey H. C. (1947) The thermodynamic properties of isotopic substances. *J. Chem. Soc.*, 562–581.

Usdowski E. and Hoefs J. (1993) Oxygen isotope exchange between carbonic acid, bicarbonate, carbonate, and water: A re-examination of the data of McCrea (1950) and an expression for the overall partitioning of oxygen isotopes between the carbonate species and water. *Geochim. Cosmochim. Acta* **57**, 3815–3818.

Usdowski E., Michaelis J., Bottcher M. E. and Hoefs J. (1991) Factors for the oxygen isotope equilibrium fractionation between aqueous and gaseous CO_2, carbonic acid, bicarbonate, carbonate, and water (19 ℃). *Z. Phys. Chem.* **170**, 237–249.

Wang L., Ruiz-Agudo E., Putnis C. V. and Putnis A. (2011) Direct observations of the modification of calcite growth morphology by Li^+ through selectively stabilizing an energetically unfavourable face. *CrystEngComm* **13**, 3962–3966.

Watkins J. M., Nielsen L. C., Ryerson F. J. and DePaolo D. J. (2013) The influence of kinetics on the oxygen isotope composition of calcium carbonate. *Earth Planet. Sci. Lett.* **375**, 349–360.

Watkins J. M., Hunt J. D., Ryerson F. J. and DePaolo D. J. (2014) The influence of temperature, pH, and growth rate on the $\delta^{18}O$ composition of inorganically precipitated calcite. *Earth Planet. Sci. Lett.* **404**, 332–343.

Watkins J. M., DePaolo D. J. and Watson E. B. (2017) Kinetic Fractionation of Non-Traditional Stable Isotopes by Diffusion and Crystal Growth Reactions. *Rev. Mineral. Geochem.* **82**, 85–125.

Wolthers M., Nehrke G., Gustafsson J. P. and Van Cappellen P. (2012) Calcite growth kinetics: Modeling the effect of solution stoichiometry. *Geochim. Cosmochim. Acta* **77**, 121–134.

Yumol L. M., Uchikawa J. and Zeebe R. E. (2020) Kinetic isotope effects during CO_2 hydration: Experimental results for carbon and oxygen fractionation. *Geochim. Cosmochim. Acta* **279**, 189–203.

Zeebe R. E. (2007) An expression for the overall oxygen isotope fractionation between the sum of dissolved inorganic carbon and water. *Geochem. Geophys. Geosyst.* **8**, 1–7.

Zeebe R. E. (2014) Kinetic fractionation of carbon and oxygen isotopes during hydration of carbon dioxide. *Geochim. Cosmochim. Acta* **139**, 540–552.

Zeebe R. E. (2020) Oxygen isotope fractionation between water and the aqueous hydroxide ion. *Geochim. Cosmochim. Acta* **289**, 182–195.

Zeebe R. E. and Wolf-Gladrow D. (2001) *CO_2 in seawater: equilibrium, kinetics, isotopes*. Elsevier Oceanography Series, Amsterdam.

Zhang H., Blanco-Ameijeiras S., Hopkinson B. M., Bernasconi S. M., Mejia L. M., Liu C. and Stoll H. (2021) An isotope label method for empirical detection of carbonic anhydrase in the calcification pathway of the coccolithophore Emiliania huxleyi. *Geochim. Cosmochim. Acta* **292**, 78–93.

Zuddas P. and Mucci A. (1998) Kinetics of calcite precipitation from seawater: II. The influence of the ionic strength. *Geochim. Cosmochim. Acta* **62**, 757–766.

Associate editor: Ruth Blake